Spatial coherence of electron bunches extracted from an arbitrarily shaped cold atom electron source

Sebastian D. Saliba, Corey T. Putkunz, David V. Sheludko, Andrew J. McCulloch, Keith A. Nugent, and Robert E. Scholten*

ARC Centre of Excellence for Coherent X-ray Science, School of Physics, The University of Melbourne, 3010, Australia

*scholten@unimelb.edu.au

Abstract: We describe the spatial coherence properties of a cold atom electron source in the framework of a quasihomogeneous wavefield. The model is used as the basis for direct measurements of the transverse spatial coherence length of electron bunches extracted from a cold atom electron source. The coherence length is determined from the measured visibility of a propagated electron distribution with a sinusoidal profile of variable spatial frequency. The electron distribution was controlled via the intensity profile of an atomic excitation laser beam patterned with a spatial light modulator. We measure a lower limit to the coherence length at the source of $l_c = 7.8 \pm 0.9\,\mathrm{nm}$.

OCIS codes: (030.0030) Coherence and statistical optics; (030.1640) Coherence; (080.5084) Phase space methods of analysis; (110.4980) Partial coherence in imaging; (140.3300) Laser beam shaping.

References and links

1. R. Henderson and P. N. T. Unwin, "Three-dimensional model of purple membrane obtained by electron microscopy," Nature **257**, 28–32 (1975).
2. B. G. Levi, "Focus on improving transmission electron microscopes starts to pay off," Phys. Today **63**, 15–19 (2010).
3. H. Ihee, V. A. Lobastov, U. M. Gomez, B. M. Goodson, R. Srinivasan, C. Y. Ruan, and A. H. Zewail, "Direct imaging of transient molecular structures with ultrafast diffraction," Science **291**, 458–463 (2001).
4. J. Cao, Z. Hao, H. Park, C. Tao, D. Kau, and L. Blaszczyk, "Femtosecond electron diffraction for direct measurement of ultrafast atomic motions," Appl. Phys. Lett. **83**, 1044 (2003).
5. B. J. Siwick, J. R. Dwyer, R. E. Jordan, and R. J. D. Miller, "An atomic-level view of melting using femtosecond electron diffraction," Science **302**, 1382–1385 (2003).
6. H. M. Quiney and K. A. Nugent, "Biomolecular imaging and electronic damage using X-ray free-electron lasers," Nat. Phys. **7**, 142–146 (2011).
7. 2.M. M. Seibert, T. Ekeberg, F. R. N. C. Maia, M. Svenda, J. Andreasson, O. Jonsson, D. Odic, B. Iwan, A. Rocker, D. Westphal, M. Hantke, D. P. DePonte, A. Barty, J. Schulz, L. Gumprecht, N. Coppola, A. Aquila, M. Liang, T. A. White, A. Martin, C. Caleman, S. Stern, C. Abergel, V. Seltzer, J.-M. Claverie, C. Bostedt, J. D. Bozek, S. Boutet, A. A. Miahnahri, M. Messerschmidt, J. Krzywinski, G. Williams, K. O. Hodgson, M. J. Bogan, C. Y. Hampton, R. G. Sierra, D. Starodub, I. Andersson, S. Bajt, M. Barthelmess, J. C. H. Spence, P. Fromme, U. Weierstall, R. Kirian, M. Hunter, R. Bruce Doak, Stefano Marchesini, Stefan P. Hau-Riege, Matthias Frank, Robert L. Shoeman, Lukas Lomb, Sascha W. Epp, Robert Hartmann, Daniel Rolles, A. Rudenko, C. Schmidt, L. Foucar, N. Kimmel, P. Holl, B. Rudek, B. Erk, A. Homke, C. Reich, D. Pietschner, G. Weidenspointner, L. Struder, G. Hauser, H. Gorke, J. Ullrich, I. Schlichting, S. Herrmann, G. Schaller, F. Schopper, H. Soltau, K.-U. Kuhnel, R. Andritschke, C.-D. Schroter, F. Krasniqi, M. Bott, S. Schorb, Da. Rupp, M. Adolph, T. Gorkhover, H. Hirsemann, G. Potdevin, H. Graafsma, B. Nilsson, H. N. Chapman, and J. Hajdu, "Single mimivirus particles intercepted and imaged with an X-ray laser," Nature **470**, 78–81 (2011).

#161202 - $15.00 USD
Received 10 Jan 2012; accepted 25 Jan 2012; published 1 Feb 2012

8. P. Piot, "Review of experimental results on high-brightness photo-emission electron sources," in *The Physics and Applications of High Brightness Electron Beams*, J. Rosenzweig, ed. (World Scientific, 2003), pp. 127–142.
9. N. de Jonge, M. Allioux, J. T. Oostveen, K. B. Teo, and W. I. Milne, "Optical performance of carbon-nanotube electron sources," Phys. Rev. Lett. **94**, 186807 (2005).
10. T. van Oudheusden, P. L. E. M. Pasmans, S. B. van der Geer, M. J. de Loos, M. J. van der Wiel, and O. J. Luiten, "Compression of subrelativistic space-charge-dominated electron bunches for single-shot femtosecond electron diffraction," Phys. Rev. Lett. **105**, 264801 (2010).
11. B. J. Claessens, S. B. van der Geer, G. Taban, E. J. D. Vredenbregt, and O. J. Luiten, "Ultracold electron source," Phys. Rev. Lett. **95**, 164801 (2005).
12. S. B. van der Geer, M. J. de Loos, E. J. D. Vredenbregt, and O. J. Luiten, "Ultracold electron source for single-shot, ultrafast electron diffraction," Microsc. Microanal. **15**, 282 (2009).
13. A. J. McCulloch, D. V. Sheludko, S. D. Saliba, S. C. Bell, M. Junker, K. A. Nugent, and R. E. Scholten, "Arbitrarily shaped high-coherence electron bunches from cold atoms," Nat. Phys. **7**, 785–788 (2011).
14. O. J. Luiten, B. J. Claessens, S. B. van der Geer, M. P. Reijnders, G. Taban, and E. J. D. Vredenbregt, "Ultracold electron sources," Int. J. Mod. Phys. A **22**, 3882–3897 (2007).
15. D. Paterson, B. E. Allman, P. J. McMahon, J. Lin, N. Moldovan, K. A. Nugent, I. McNulty, C. T. Chantler, C. C. Retsch, T. H. K. Irving, and D. C. Mancini, "Spatial coherence measurement of X-ray undulator radiation," Opt. Commun. **195**, 79–84 (2001).
16. K. A. Nugent, "Coherent methods in the x-ray sciences," Adv. Phys. **59**, 1–99(99) (2010).
17. J. L. Roberts, C. D. Fertig, M. J. Lim, and S. L. Rolston, "Electron temperature of ultracold plasmas," Phys. Rev. Lett. **92**, 253003 (2004).
18. W. H. Carter and E. Wolf, "Coherence and radiometry with quasihomogeneous planar sources," J. Opt. Soc. Am. **67**, 785 (1977).
19. E. Wolf, "Coherence and radiometry," J. Opt. Soc. Am. **68**, 6–17 (1978).
20. J. J. Lin, D. Paterson, A. G. Peele, P. J. McMahon, C. T. Chantler, K. A. Nugent, B. Lai, N. Moldovan, Z. Cai, D. C. Mancini, and I. McNulty, "Measurement of the spatial coherence function of undulator radiation using a phase mask," Phys. Rev. Lett. **90**, 074801 (2003).
21. T. Gallagher, *Rydberg Atoms* (Cambridge University Press, 1994).
22. O. J. Luiten, S. B. van der Geer, M. J. de Loos, F. B. Kiewiet, and M. J. van der Wiel, "How to realize uniform three-dimensional ellipsoidal electron bunches," Phys. Rev. Lett. **93**, 094802 (2004).
23. M. A. Alonso, "Wigner functions in optics: describing beams as ray bundles and pulses as particle ensembles," Adv. Opt. Photon. **3**, 272–365 (2011).
24. J. L. Hanssen, S. B. Hill, J. Orloff, and J. J. McClelland, "Magneto-optical-trap-based, high brightness ion source for use as a nanoscale probe," Nano Lett. **8**, 2844–2850 (2008).
25. P. Gupta, S. Laha, C. E. Simien, H. Gao, J. Castro, T. C. Killian, and T. Pohl, "Electron-temperature evolution in expanding ultracold neutral plasmas," Phys. Rev. Lett. **99**, 075005 (2007).
26. R. Côté, T. Pattard, and M. Weidemüller, "Special issue on Rydberg physics," J. Phys. B **38**, (2005).

1. Introduction

Electron probes are an important tool for nanometre scale investigations, for example the determination of membrane protein structures [1]. Improvements in electron sources have enabled increased spatial and temporal resolution beyond optical alternatives [2]. In particular, ultrafast electron diffraction (UED) is an emerging technique for obtaining atomic-level structural dynamics at sub-picosecond timescales, such as atomic motion and phase transitions [3–5]. Ultrafast diffraction also has the potential to capture images before sample damage occurs, essential to imaging biological specimens with sub-nanometre resolution [6,7].

Carbon nanotube (CNT) field emitters are currently the brightest available electron sources, though must operate at low currents to avoid Coulomb expansion and are therefore not suitable for ultrafast imaging [8,9]. Conventional photoemission sources use high energy laser pulses to generate hot electrons at high current. Recently, sub-100 fs 0.25 pC electron bunches have been extracted from a photoemission source, enabling demonstration of single-shot diffraction from a crystalline gold foil [10].

Electron bunches extracted from cold atoms provide a new and intrinsically different source for UED imaging [11–13]. In a cold atom electron source (CAES), electrons are extracted by photoionization of laser cooled and trapped atoms (temperature $T < 100\,\mu$K). The predicted upper limit to transverse normalized brightness for these sources is comparable to that of CNT

#161202 - $15.00 USD Received 10 Jan 2012; accepted 25 Jan 2012; published 1 Feb 2012

emission sources, but with significantly higher electron flux [14].

Conventional electron sources are initially incoherent, and useful coherence is obtained only as a consequence of propagation, described by the van Cittert-Zernike theorem. A CAES produces very low temperature electrons ($T < 15\,\mathrm{K}$ [13]) with small initial transverse momentum spread, and consequently the transverse spatial coherence is large *at the source*. As with conventional electron sources, the CAES coherence can then be further enhanced by propagation, and the flux of a CAES can be many orders of magnitude greater than single-atom field emitters. The CAES therefore has promising properties desirable for diffractive imaging, including sufficient intrinsic transverse spatial coherence for imaging whole biomolecules coupled with the potential for high brightness.

An electron bunch extracted from a CAES has the properties of a partially coherent quasi-homogeneous wavefield. While the temperature of these cold electron bunches has previously been measured and a transverse spatial coherence length inferred [13], in this paper we directly measure the transverse spatial coherence by mapping out the form of the coherence function, thus confirming the basic property which makes these new sources important for diffractive imaging. We measure the visibility of a propagated electron distribution with a sinusoidal profile, created at the source by directly modifying the excited state atomic distribution [13]. This profile can be rapidly varied to allow measurements over a wide range of spatial frequencies. The variation in the visibility of the propagated electron profile with spatial frequency is shown to relate to the coherence function in close analogy to the visibility of a two-slit interference fringe pattern commonly used to characterize source coherence [15,16].

2. A cold atom electron source

2.1. Experimental description

In our experiments, approximately $10^9\,\mathrm{Rb}^{85}$ atoms in a magneto-optical trap ($T = 70\,\mu\mathrm{K}$) were excited from the $5S_{1/2}(F = 3)$ ground state to the $5P_{3/2}(F' = 4)$ excited state using a laser of wavelength 780 nm (Fig. 1). The intensity profile of the excitation laser beam was shaped using a phase-only spatial light modulator (SLM) to selectively excite a desired density distribution of atoms within the Rb cloud [13]. The shaped, excited atom distribution was photoionized using a 5 ns 480 nm wavelength laser pulse, spatially uniform to 3% across the cloud. The electrons were accelerated in a uniform electric field ($F = 40\,\mathrm{kV/m}$, distance 2.5 cm, final energy 1 keV) parallel to the excitation laser and propagated 22 cm in a null field. The spatial distribution of the electron pulse was observed on a phosphor screen attached to a micro channel plate (MCP) charge amplifier.

2.2. Modelling a cold atom electron source

To model the CAES, we first assume the initial electron bunch has a Maxwellian momentum distribution described by

$$f(\mathbf{p}) = \left(\frac{1}{2\pi m k_B T}\right)^{3/2} \exp\left[-\frac{|\mathbf{p}_\perp|^2 + p_{||}^2}{2 m k_B T}\right] \tag{1}$$

where m is the electron mass, k_B is the Boltzmann constant, T is the electron temperature, and the electron momentum is separated into a 2D component perpendicular to the propagation axis, $\mathbf{p}_\perp$, and a component parallel to the propagation axis, $p_{||}$. The transverse momentum spread $\sigma_{p_\perp} = \sqrt{m k_B T}$ is small due to the very low electron temperature (Fig. 2), fundamentally limited by intrinsic heating processes immediately following ionization [17]. The electrons were accelerated along the propagation axis by electric field F, imparting an additional momentum component p_F. Since $p_F \gg p_{||}$, we regard the electron distribution as having a

#161202 - $15.00 USD Received 10 Jan 2012; accepted 25 Jan 2012; published 1 Feb 2012

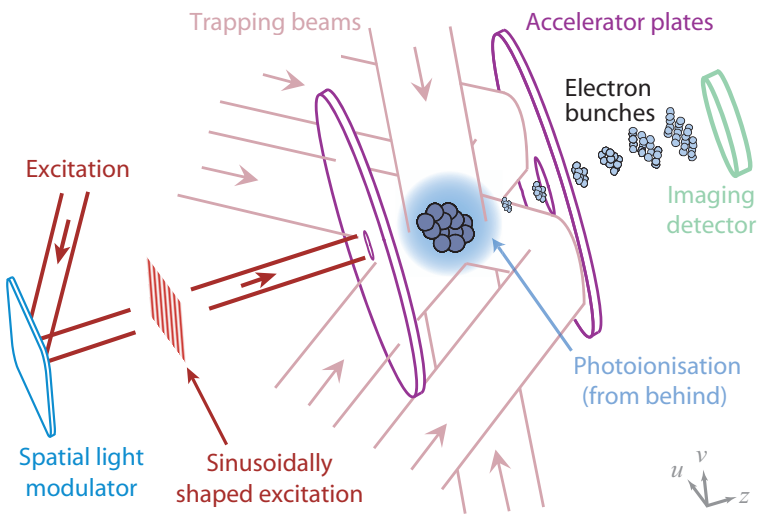

Fig. 1. Schematic of the cold atom electron source, showing the cold atom magneto-optic trap, electrostatic accelerator plates, spatial light modulator (SLM) and detector. The atom cloud was excited by a 780 nm laser along the electron acceleration axis. The excitation laser was shaped using the SLM to select a spatial profile of cold atoms with a sinusoidal variation in one transverse direction and a constant amplitude in the other transverse direction (see also Fig. 3). A 480 nm laser was tuned to ionize atoms from the excited state prior to extraction in a static electric field. The electrons were detected on a phosphor screen attached to a micro channel plate charge amplifier.

well-defined momentum component in this direction, such that the bunch is analogous to a quasi-monochromatic paraxial optical wavefield [18].

The propagated electron bunch phase-space density for the transverse components, $W(\mathbf{r},\mathbf{p}_\perp)$, can therefore be described by

$$W(\mathbf{r},\mathbf{p}_\perp) = f(\mathbf{p}_\perp)I(\mathbf{r}) \tag{2}$$

where $I(\mathbf{r})$ describes the spatial intensity distribution of the source in the plane perpendicular to the propagation axis and Eq. (1) has been separated into transverse and parallel propagation components $f(\mathbf{p}) = f(\mathbf{p}_\perp)f(p_{||})$ with

$$f(\mathbf{p}_\perp) = f_0 \exp\left(-\frac{|\mathbf{p}_\perp|^2}{2mk_BT}\right) \tag{3}$$

and $f_0 = 1/2\pi mk_BT$.

The quasi-homogeneous model (QHM) treats the source as a series of mutually incoherent point radiators each radiating into a small angular distribution (see Fig. 2). Conceptually, the effective source size at some point in the propagated electron beam is defined by the momentum spread (temperature) at the source, and not by the physical size of the source or electron beam. A QHM is appropriate for a source with short correlation length [16], such as the CAES. The correlations in the field between two points $\mathbf{r}_1$ and $\mathbf{r}_2$ can then be described by the mutual optical intensity (MOI) for a quasi-homogeneous source

$$J(\mathbf{r},\mathbf{x}) = I(\mathbf{r})\gamma(\mathbf{x}) \tag{4}$$

where $\mathbf{r} = (\mathbf{r}_1 + \mathbf{r}_2)/2$ and $\gamma(\mathbf{x})$ describes the correlations between the electrons as a function of separation $\mathbf{x} = \mathbf{r}_1 - \mathbf{r}_2$. The QHM naturally leads to the limit of a completely incoherent

#161202 - $15.00 USD
Received 10 Jan 2012; accepted 25 Jan 2012; published 1 Feb 2012

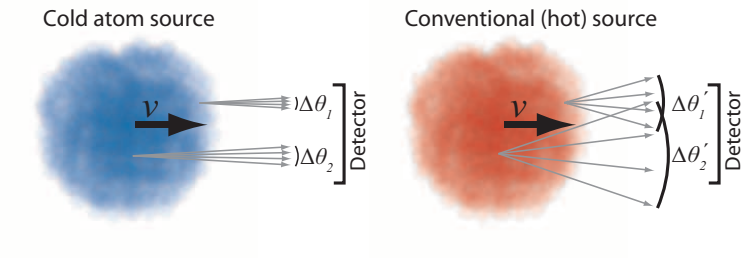

Fig. 2. Schematic of the quasi-homogeneous model as it applies to the cold atom electron source (left). Each electron has the same finite and uniform angular spread $\Delta\theta$ and hence angular distribution. Conventional sources (right) have a much larger associated angular spread with $\Delta\theta' \gg \Delta\theta$ such that it is not possible to identify the origin of a detected electron.

source by substituting a delta function for $\gamma(\mathbf{x})$. The properties of quasi-homogeneous sources are discussed in detail in Refs. [16,18,19].

The MOI is related to the phase-space distribution via [19]:

$$J\left(\mathbf{r}+\frac{\mathbf{x}}{2},\mathbf{r}-\frac{\mathbf{x}}{2}\right)=\int W(\mathbf{r},\mathbf{p}_\perp)\exp\left[i\frac{\mathbf{x}\cdot\mathbf{p}_\perp}{h}\right]d\mathbf{p}_\perp. \tag{5}$$

Combining Eqs. (1), (2) and (5) and evaluating the integral, we identify a Gaussian form of the coherence function

$$\gamma(\mathbf{x})=\exp\left[-\frac{|\mathbf{x}|^2}{2l_c^2}\right] \tag{6}$$

where $l_c=h/\sqrt{mk_BT}$ is identified as the coherence length of the quasi-homogeneous source, and is related to the transverse momentum spread of the electrons via $l_c=h/\sigma_{p_\perp}$. Gaussian forms for the coherence function $\gamma(\mathbf{x})$ are common [18,19] and have been investigated extensively, for example for modern x-ray sources [15,20]. The initial momentum spread $\sigma_{p_\perp}$, and therefore the coherence length, depends only on the electron temperature and are independent of the axial acceleration energy imparted to the electron bunch. For a CAES, the electron temperature is determined by the excess electron energy ΔE, which is primarily the energy difference between the photoionization laser photon energy and the ionization threshold of the atoms in an ambient electric field [21]. At high excess energy, the electron angular distribution broadens and for an electron at the detector we can no longer determine the trajectory from the source. A high excess ionization energy thus corresponds to the incoherent source limit, $\gamma(\mathbf{x})\rightarrow\delta(\mathbf{x})$.

The standard methods of optical coherence theory may be adapted for the propagation of a partially coherent electron field. We make the paraxial approximation, and the intensity of the electron field at a distance z is then given by [16]

$$I(\mathbf{r},z)=\frac{k^2}{4\pi^2z^2}\int J(\mathbf{r}',\mathbf{x}')\exp\left[i\frac{k}{z}\mathbf{x}'\cdot(\mathbf{r}'-\mathbf{r})\right]d\mathbf{r}'d\mathbf{x}' \tag{7}$$

where $k=2\pi/\lambda$ and λ is the de Broglie wavelength of the electrons.

3. Measuring the spatial coherence function of a cold atom electron source

3.1. Arbitrarily shaped electron bunches

A unique feature of the CAES is that it allows virtual 'masking' of the electrons. We can alter the initial electron spatial distribution shot-to-shot by changing the SLM phase mask (see

#161202 - $15.00 USD
Received 10 Jan 2012; accepted 25 Jan 2012; published 1 Feb 2012

Fig. 1). The electron bunches can also be shaped along the propagation direction by control of the orthogonal photoionization laser beam profile [13]. This approach could be used to produce 'pancake' bunches that evolve naturally to form ideal uniform ellipsoidal density distributions to alleviate coherence loss due to non-linear Coulomb interactions within the bunch [14, 22].

We impose a sinusoidal distribution on the cold atom cloud so that the MOI (Eq. (4)) becomes

$$J(\mathbf{r},\mathbf{x}) = \frac{I_0}{2}\left(1+\sin\left(2\pi\frac{u}{d}\right)\right)\exp\left[-\frac{|\mathbf{x}|^2}{2l_c^2}\right] \tag{8}$$

where d is the period of the sinusoid and $\mathbf{r} \equiv (u,v)$, so that

$$I(\mathbf{r},z) = \frac{k^2}{4\pi^2 z^2} I_0 \left(1+\exp\left[-\frac{\lambda^2 z^2}{d^2 l_c^2}\right]\sin\left(2\pi\frac{u}{d}\right)\right). \tag{9}$$

The visibility measured at the detector, $\mathscr{V} \equiv (I_{\max}-I_{\min})/(I_{\max}+I_{\min})$, then reduces to

$$\mathscr{V} = \exp\left[-\frac{(1/d)^2}{l_c^2/\lambda^2 z^2}\right]. \tag{10}$$

Equation (9) describes a loss of visibility in a form that is mathematically identical to that obtained for a Young's two-slit experiment in which the slits are placed in the source plane and the detector is sufficiently distant to produce the observed fringe frequency. This correspondence is not coincidental as can be seen when coherence is described in terms of the Wigner quasi-probability distribution (see, for example, Refs. [16] and [23]). In both forms of the experiment, the coherence is determined from the visibility of the fringe pattern. In the form here, it is straightforward to vary the fringe spacing using the SLM and to probe the coherence function $\gamma(\mathbf{x})$ at varying fringe frequencies, which is precisely equivalent to varying the slit separation.

3.2. Experimental method

The sinusoidal electron bunch signal incident on the MCP/phosphor screen was imaged with a CCD camera (Fig. 3). The images were integrated along v to improve the signal to noise ratio, and the line profiles were then normalized to an electron distribution without sinusoidal variation. Changes in the overall size of the electron bunch, caused by the inhomogeneous electric field at the accelerator aperture exit acting as a Davisson-Calbick lens [24], do not affect the sinusoidal visibility. Figure 3 shows an example of a fit of Eq. (9) to a measured electron distribution for a single spatial frequency. The uncertainty in each visibility measurement was calculated using the error matrix from the non-linear least squares fit.

3.3. Results

A Gaussian fit to the visibility as a function of spatial frequency, shown in Fig. 4, yields the transverse spatial coherence length, l_c (Eq. (10)). The propagation distance $z = 234 \pm 15$ mm is determined from a fit to electron and ion time of flight data and the electron de Broglie wavelength $\lambda = 39 \pm 1$ pm is calculated from the imparted bunch energy. The resulting transverse coherence length is $l_c = 7.8 \pm 0.9$ nm with an inferred electron temperature of $T = 14 \pm 2$ K. The coherence length measurement here is a lower limit as the reduction in visibility cannot be exclusively attributed to coherence effects. For example, a small distortion of the parallel sinusoidal pattern evident in Fig. 3 is due to non-uniform electric and magnetic fields during propagation [13].

Figure 5 shows the variation of coherence length with excess ionization energy, T_L; that is, the additional heating above threshold, governed by the photoionization laser wavelength. The electron temperature is further increased by T_0 due to additional internal heating processes

#161202 - $15.00 USD Received 10 Jan 2012; accepted 25 Jan 2012; published 1 Feb 2012

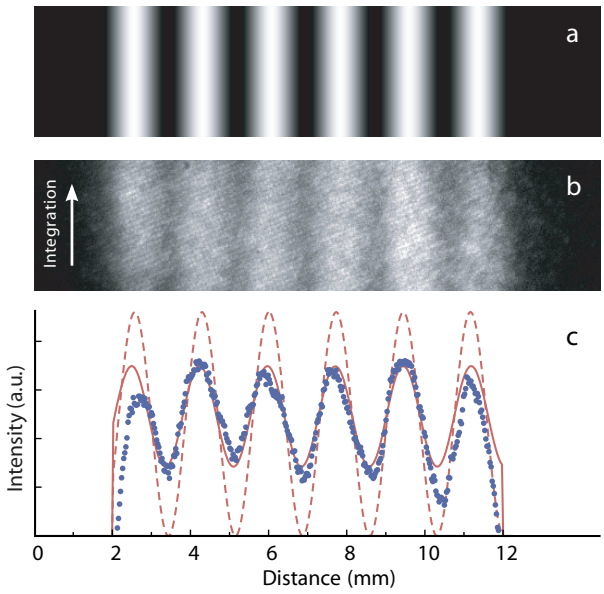

Fig. 3. (a) Desired excitation laser beam intensity profile used to create the spatial light modulator phase mask. (b) Image of resulting shaped electron bunch on the phosphor screen. (c) Integrated line profile of the calculated fully coherent electron distribution (red dashed), the recorded electron image (blue points), and a fit to the recorded data based on Eq. (9) (red solid).

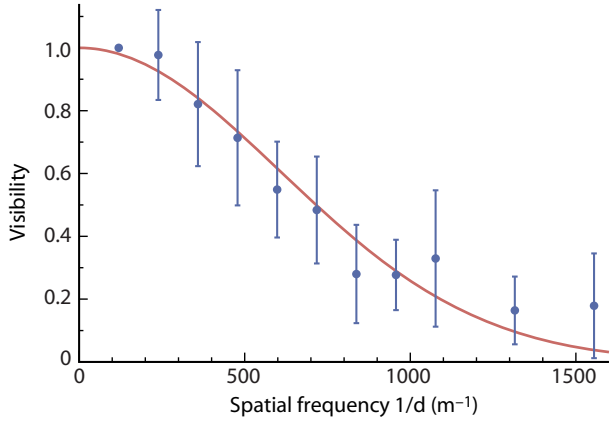

Fig. 4. Visibility of electron bunch pattern as a function of spatial frequency, with a Gaussian fit to the visibility function resulting in $l_c = 7.8 \pm 0.9$ nm. The systematic uncertainty in measuring d was 3%.

#161202 - $15.00 USD
Received 10 Jan 2012; accepted 25 Jan 2012; published 1 Feb 2012

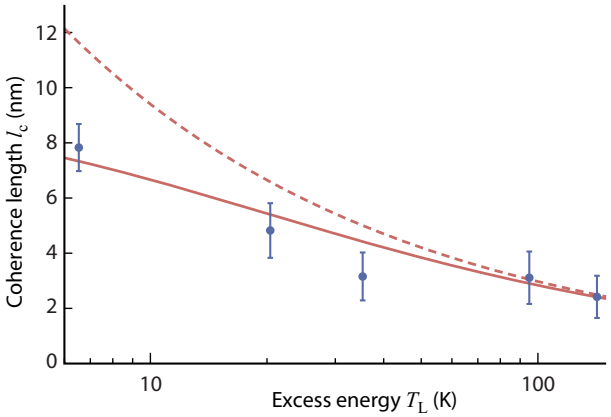

Fig. 5. Variation of coherence length with excess ionization energy. The red dashed line shows how the coherence length varies with no additional disorder induced heating ($T_0 = 0\,\mathrm{K}$). The solid line is a least-squares fit to temperature-varying coherence length with heating of $T_0 = 9.9 \pm 3\,\mathrm{K}$.

immediately following ionization [25]. The final electron temperature is then $T_L + T_0$ and the coherence length is expected to vary as $l_c = h/\sqrt{mk_B(T_L + T_0)}$. The wavelength of the ionization laser was varied from 481.727 nm to 478.470 nm, equivalent to excess energy of $T_L = 6.5\,\mathrm{K}$ to 142.1 K. The resulting increase in bunch temperature is apparent as a decrease in coherence length. From a fit to the coherence length with free parameter T_0 (solid line, Fig. 5) we find $T_0 = 9.9 \pm 3\,\mathrm{K}$. Ionization with zero excess energy ($T_L = 0\,\mathrm{K}$) could be achieved by tuning the ionization laser wavelength and accelerating electric field to a Rydberg state resonance [26]. The resulting coherence length would then be $l_c = 9.5\,\mathrm{nm}$, in close agreement to previous indirect estimates [13].

4. Conclusion

Temperatures as low as $T < 10 \pm 5\,\mathrm{K}$ have been measured for a CAES [13] indicating a characteristic coherence length of $l_c > 10 \pm 3\,\mathrm{nm}$. A coherence length of 10 nm is already sufficient *at the source* for imaging small biomolecules such as bacteriorhodopsin where the unit cell length is of order 10 nm. In contrast, photoemission electron sources with electron bunch temperatures of order $T = 10^4\,\mathrm{K}$ have an associated coherence length of $l_c = 0.3\,\mathrm{nm}$.

This paper has provided a framework for describing the propagation of partially coherent electron bunches extracted from a cold atom electron source: a critical requirement for realization of coherent diffractive imaging using a CAES. The arbitrary bunch shaping capability of the CAES has enabled a convenient and flexible method for measuring the transverse spatial coherence of the electron bunches. The measured coherence length of the CAES and the potential for high brightness are promising for application to coherent diffractive imaging of biological and other nanocrystals.

Acknowledgments

The authors acknowledge the support of the Australian Research Council through the Federation Fellowship program and ARC Discovery Project DP1096025.

#161202 - $15.00 USD
Received 10 Jan 2012; accepted 25 Jan 2012; published 1 Feb 2012